Application of YIQ Color Model for Color Pattern Recognition with Shifted and Rotated Training Images in Optoelectronic Correlator

Yachu Hsieh, Chulung Chen*, Hsinyi Chen, Yiting Tsai

***Abstract*—This research uses multi-channel system for chromatic pattern recognition, which reduces the size requirement of liquid crystal device. We transform a color image into three YIQ color space components. Via the utilization of Mach-Zehnder joint transform correlator, the minimum average correlation energy method, shifted training images, and computation, we will obtain the reference functions by the minimum sidelobe energy technique and record the relevant data. It is found that the sidelobe energy drops substantially.**

***Index Terms*—Minimum average correlation energy, training image, YIQ color space, Mach-Zehnder joint transform correlator, liquid crystal spatial light modulator.**

I. Introduction

Real time joint transform correlator (JTC) [1] is an attractive tool for pattern recognition. It can perform correlation of two functions to realize the aim. Later, non-zero order JTC (NOJTC) [2-4] was utilized to remove the zero order term. High correlator peak intensity and small sidelobe energy were obtained. Chen et al. [5-10] utilized the minimum average correlation energy (MACE) method based on Lagrangian method to obtain the reference function. The Mach-Zehnder JTC (MZJTC) [11,12] can accomplish the removed zero term processing in only one step directly. In this paper, the sytem was based on MZJTC, we obtain the reference functions by cross correlation optimization technique and find the minimum sidelobe energy by shifted training images. In the paper, we will use MACE as well as shifted training images [13,14] to study the performance for image recognition in the MZJTC system.

II. Analysis

RGB color model [15-17] is used widely and is easy to understand. It consists of the red, green and blue respectively. However, RGB color model is not the most suitable color model on many applications. In this research, the system is based on YIQ color model [18]. Y means luminance that represents the achromatic (black and white) image without any color. I and Q are the two chrominance components. I is deviations from orange-luminance to cyan-luminance and Q is deviations from purple-luminance to chartreuse–luminance. It transform RGB source into one luminance and two chrominance components by linear conversion. The transformation from RGB to YIQ is shown below.

$$\begin{bmatrix} Y \\ I \\ Q \end{bmatrix} = \begin{bmatrix} 0.299 & 0.587 & 0.114 \\ 0.596 & -0.275 & -0.321 \\ 0.212 & -0.523 & 0.311 \end{bmatrix} \begin{bmatrix} R \\ G \\ B \end{bmatrix}. \quad (1)$$

The structure of optical correlator [12,13] is shown in Fig. 1. A laser is used to be the light source. In the beginning, we define the position functions of reference and target images on the two input planes. There are three grayscale images h_y, h_i and h_q, corresponding to the y, i and q channels of the reference image. Analogously, another three grayscale images t_y, t_i and t_q, are matched to the Y, I and Q channels of the target image. The arrangement of input plane in RLCSLM1 and RLCSLM2 are shown in Figs. 2 and 3. The reference and target image channels placed on the RLCSLM1 and RLCSLM2 respectively can be expressed as

$$h = \sum_{m=1}^{3} h_m\left(x + d, y + a_m\right), \quad (2)$$

and

$$t = \sum_{n=1}^{3} t_n\left(x - d, y + a_n\right). \quad (3)$$

Here d is the distance of either the reference image or target image channel away from the horizontal axis; h represents the position function of reference image at RLCSLM1; t represents the position function of target image at RLCSLM2. After coming out of RLCSLM1 and RLCSLM2, the two collimated light will take the information and be Fourier transformed by Fourier lens (FLs). Both lights encounter fractional reflection and transmission at BS3. Joint transform power spectrums (JTPSs) of two light fields will be detected by CCD1 and CCD2. The summation of spectra on CCD1 is

$$E_1(u,v) = \sum_{m=1}^{3} \tau_1 \cdot H_m(u,v) \cdot e^{j2\pi(du + a_m v)} + \sum_{n=1}^{3} \gamma_1 \cdot T_m(u,v) \cdot e^{-j2\pi(du - a_n v)}. \quad (4)$$

On the other hand, the summation of spectra on CCD2 is

Manuscript received July 29, 2013.. This work was supported by the National Science Council in Taiwan, under Grant No. NSC 102-2221-E-155 -082- MY2

Yachu Hsieh is with the institute of Photonics Engineering, Yuan Ze university, 135 Yung Tung Road, Taoyuan 32026, Taiwan.

Chulung Chen is with the institute of Photonics Engineering, Yuan Ze university, 135 Yung Tung Road, Taoyuan 32026, Taiwan. (Corresponding author. Phone: +886-3-4638800 ext 7513; Fax: +886-3-4639355; E-mail: chulung@saturn.yzu.edu.tw).

$$E_2(u,v) = \sum_{m=1}^{3} \gamma_1 \cdot H_m(u,v) \cdot e^{j2\pi(du+a_m v)} + \sum_{n=1}^{3} \tau_2 \cdot T_m(u,v) \cdot e^{-j2\pi(du-a_n v)}. \quad (5)$$

We connect the outputs of the CCD1 and CCD2 to the electronic subtractor (ES) to remove the zero order term as follows.

$$\begin{aligned} I_s(u,v) &= |E_2(u,v)|^2 - |E_1(u,v)|^2 \\ &= (|\gamma_1|^2 - |\tau_1|^2) \cdot \sum_{m=1}^{3}\sum_{m'=1}^{3} H_m(u,v)\, H^*{}_{m'}(u,v) \cdot e^{j2\pi(z_m - z_{m'})v} \\ &+ (|\tau_2|^2 - |\gamma_2|^2) \cdot \sum_{n=1}^{3}\sum_{n'=1}^{3} T_n(u,v)\, T^*{}_{n'}(u,v) \cdot e^{j2\pi(z_n - z_{n'})v} \\ &+ (\tau_2\gamma_1{}^* - \tau_1{}^*\gamma_2) \cdot \sum_{m=1}^{3}\sum_{n=1}^{3} H_m(u,v)\, T^*{}_n(u,v) \cdot e^{j2\pi[(z_m - z_n)v + 2du]} \\ &+ (\tau_2{}^*\gamma_1 - \tau_1\gamma_2{}^*) \cdot \sum_{m=1}^{3}\sum_{n=1}^{3} H^*{}_m(u,v)\, T_n(u,v) \cdot e^{-j2\pi[(z_m - z_n)v + 2du]} \end{aligned} \quad (6)$$

Using the Stokes relations from optics knowledge, we obtain the equation $\gamma_2 = -\gamma_1$ 、$|\gamma_1| = |\tau_1|$ and $|\gamma_2| = |\tau_2|$, then rewrite the Eq. (7) as

$$I_s = 2|\tau_2\gamma_1{}^* - \tau_1{}^*\gamma_2| \cdot \sum_{m=1}^{3}\sum_{n=1}^{3} |H_m(u,v)||T_n(u,v)| \cdot cos\{2\pi[(a_m - a_n)v + 2du] + \theta + \theta_{H_m}(u,v) - \theta_{T_n}(u,v), \quad (7)$$

where θ is the phase of $\tau_2\gamma_1{}^* - \tau_1{}^*\gamma_2$, θ_{H_m} and θ_{T_n} denote the phase of $|H_m(u,v)|$ and $|T_n(u,v)|$, respectively. The zero order term is removed. I_s is called Mach-Zehnder JTPS (MZJTPS). Then we send the MZJTPS to RLCSLM3. With inverse Fourier transform by FL3, the cross-correlation output will be obtained in CCD3 as follows:

$$o(x,y) = \sum_{m=1}^{3}\sum_{n=1}^{3} c_{mn}(-x,-y) \otimes \delta(x + 2d, y - a_m + a_n) e^{(-j\theta)} + \sum_{m=1}^{3}\sum_{n=1}^{3} c^*{}_{mn}(x,y) \otimes \delta(x - 2d, y + a_m - a_n) e^{(j\theta)}. \quad (8)$$

Here the symbols $\otimes$ and $\circ$ denote correlation and convolution operations, respectively.

III. Numerical Results

In this research, we choose a colorful fish pattern to be our original color target image, as shown in Fig. 4. The image has 64 × 64 pixels. First, we transform a color image into three YIQ color space components. It is shown in Fig. 5. Then, three components are rotated angles from 5° to 360° (in step of 5°) and shifted (x = -5 to x = 5 in the horizontal direction, the interval is 1 pixel, y = -5 to y = 5 in the vertical direction, the interval is 1 pixel) at the same time. The reference images are synthesized by the training images. Subsequently, we utilize training set images with different rotation angles to be the target images for the image recognition test. We obtain the reference functions of the minimum sidelobe energy and record the relevant data. It is found that the sidelobe energy drops substantially. The desired peak can be detected and sidelobes are diminished. One example is shown in Fig. 6. In contrast with the unshifted training images, the sidelobe energy for shifted training images decreases by 60.9%, as shown in Fig. 7. We also record the results of PSR for each target image and compare the results of between original and shifted. Average PSR value increases by 1.22 times, as shown in Fig. 8.

IV. Conclusion

In this work, via the utilization of MZJTC, the minimum average correlation energy method, shifted training images, and computation. This system could remove the zero order term in only one step. We will obtain the reference functions of the minimum sidelobe energy. The result in the thesis are obviously shown and indicate ideal performance as anticipated.

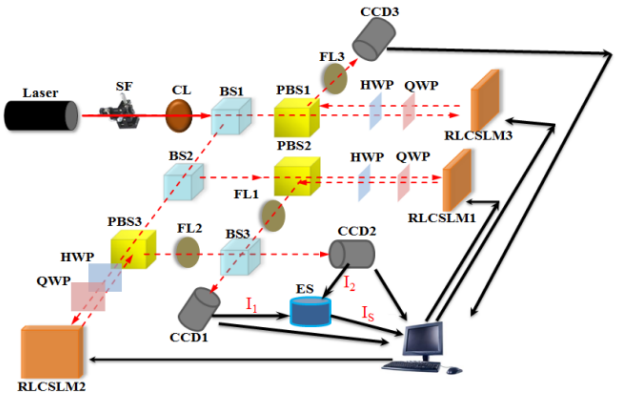

Fig.1 The structure of MZJTC system.

ISBN: 978-988-19253-2-9
ISSN: 2078-0958 (Print); ISSN: 2078-0966 (Online)

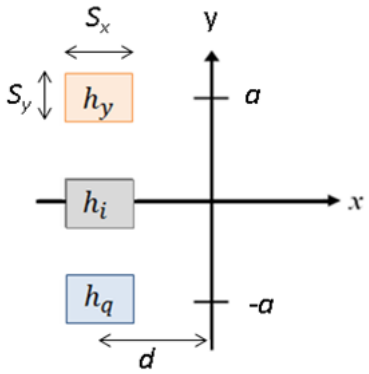

Fig. 2 Arrangement of RLCSLM1 for reference channels

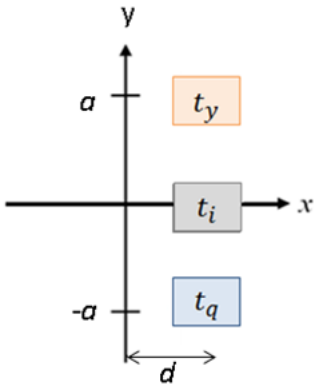

Fig. 3 Arrangement of RLCSLM1 for target channels

Fig.4 The original target image.

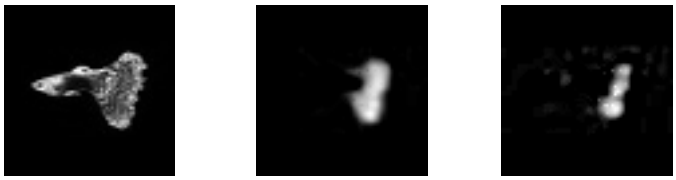

Fig.5 Y (left), I (middle) and Q (right) components of target image.

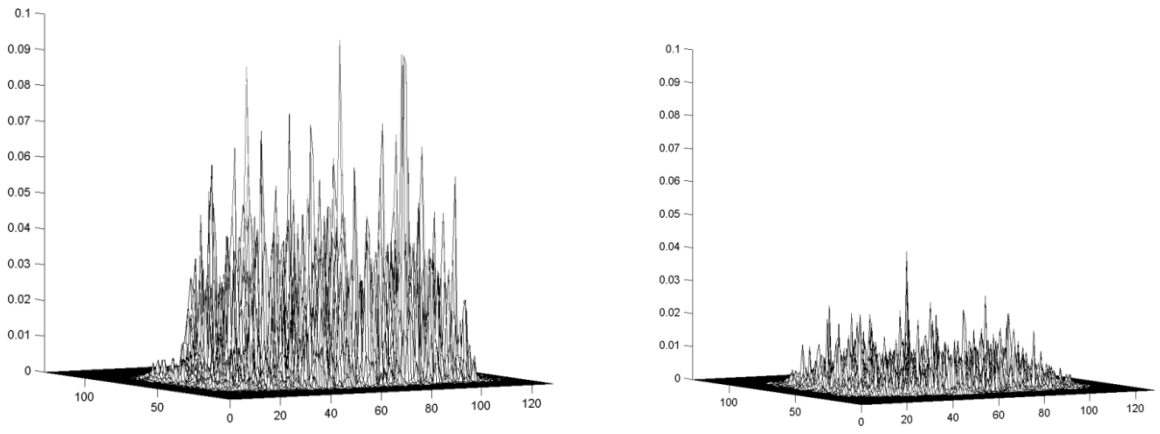

Fig.6 Example of comparison of the sidelobes between the original and improved training data base (correlation peak is removed for ease of observation)

ISBN: 978-988-19253-2-9
ISSN: 2078-0958 (Print); ISSN: 2078-0966 (Online)

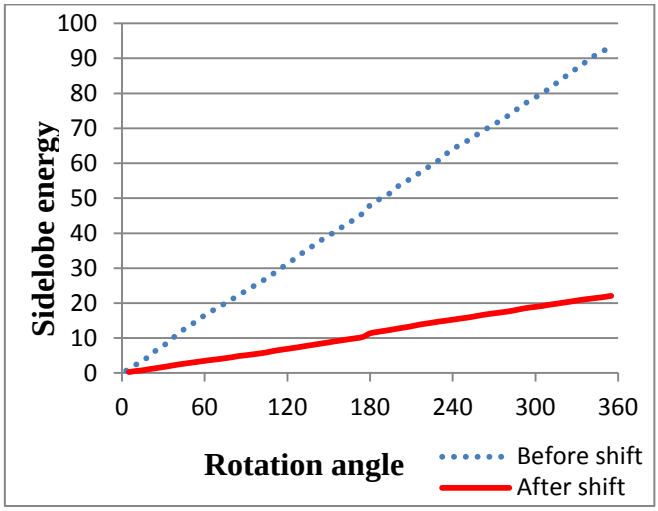

Fig.7 Sidelobe energy versus rotation angle

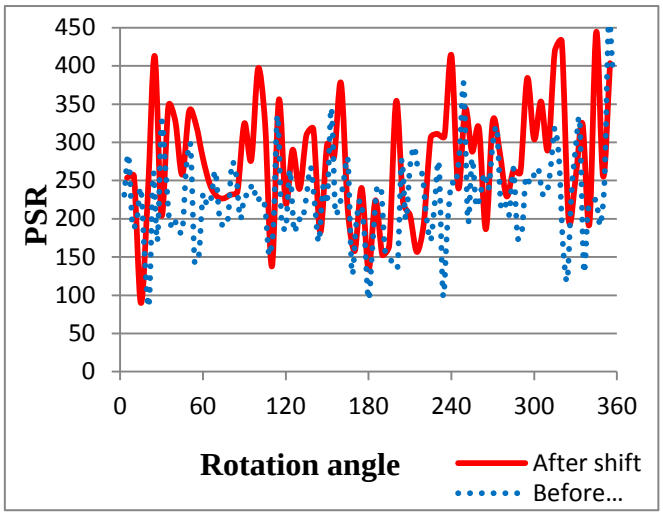

Fig.8 PSR versus rotation angle

REFERENCES

[1] F. T. S. Yu and X. J. Lu, "A real-time programmable joint transform correlator, " Opt. Commun., vol. 52, pp. 10-16, 1984

[2] F. Cheng, et al., "Removal of intra-class associations in joint transform power spectrum," Opt. Commun., vol. 99, pp. 7-12, 1993.

[3] S. Jutamulia and D. A. Gregory, "Soft blocking of the dc term in Fourier optical systems," Opt. Eng., vol. 37, pp. 49-51, 1998.

[4] G. S. Pati and K. Singh, "Illumination sensitivity of joint transform correlators using differential processing: computer simulation and experimental studies," Opt. Commun., vol. 147, pp. 26-32, 1998.

[5] C. Chen, J. Fang, "Cross-correlation peak optimization on joint transform correlators," Opt. Commun., vol. 178, pp. 315-322, 2000.

[6] C. Chen, "Minimum-variance nonzero order joint transform correlators," Opt. Commun., vol. 182, pp. 91-94, 2000

[7] C. Chen, "Correlation peak variance minimization for nonzero order joint transform correlators in noise," Microw. Opt. Techn. Lett., vol. 29(3), pp. 190-192, 2001.

[8] C. Chen, J. Fang, S. Yin, "Optimized synthetic aperture radar image detection with nonzero order joint transform correlators," Microw. Opt. Techn. Lett., vol. 26(5), pp. 312-316, 2000.

[9] C. Chen, J. Fang, "Synthetic aperture radar image recognition by constrained joint transform correlators," Optik, vol. 112(3), pp. 125-130, 2001.

[10] J. Fang, C. Chen, "Chinese seal imprint recognition by joint transform correlators," Opt. Eng., vol. 40(10), pp. 2159-2164, 2001.

[11] C. Chen, C. Chen, C. Lee, and C. Chen, "Constrained optimization on the nonzero-order joint transform correlator constructed with the Mach-Zehnder configuration," Opt. Commun., vol. 231, pp. 165-173, 2004.

[12] C. Lee, C. Chen, "A Mach-Zehnder nonzero order joint transform correlator for aircraft pattern recognition," Microw. Opt. Techn. Lett., pp. 1290-1293, vol. 48(7), 2006.

[13] C. Chen, C. Chen, "Decrease of sidelobe energy by shifts in original training images for synthetic aperture radar image recognition," Microw. Opt. Techn. Lett., vol. 41(3), pp. 241-244, 2004.

[14] C. Chen, C. Chen, "Modification of training images for the optimisation of the nonzero order joint transform correlator," J. Mod. Opt., vol. 52, pp. 21-32, 2005.

[15] C. Wu, C. Chen, "Performance comparison between multi-channel polychromatic and conventional joint transform correlators," Opt. Eng., vol. 42(6), pp. 1758-1765, 2003.

[16] C. Chen, C. Wu, "Polychromatic pattern recognition using the non-zero order joint transform correlator with cross-correlation peak optimisation," J. Mod. Opt., vol. 50(9), pp. 1353-1364, 2003.

[17] C. Chen, C. Chen, C. Lee, C. Chen, "Color face recognition with liquid crystal spatial light modulators," Microw. Opt. Techn. Lett., pp. 234-237, vol. 42(3), 2004.

[18] W. Wu, C. Chen, "Color blindness plate recognition with a YIQ multi-channel non-zero order joint transform correlator," Microw. Opt. Techn. Lett., vol. 37(5), pp. 343-347, 2003.

ISBN: 978-988-19253-2-9
ISSN: 2078-0958 (Print); ISSN: 2078-0966 (Online)